HiSST: 3rd International Conference on
High-Speed Vehicle Science & Technology
14–19 April 2024, Busan, Korea

The Combined Effects of Large-Scale Roughness and Mass Injection in Hypersonic Flow

Wesley J Condren[1], Raghul Ravichandran[1], Anthony Finnerty[1], Chris Hambidge[1], Matthew McGilvray[1]

Abstract

This paper presents an experimental study into the combined effects of large scale surface roughness and blowing. This represents the transfer of pyrolysis gases through the surface of an ablative. The experiments were conducted in the High Density Tunnel at the University of Oxford where a micro-porous transpiration cooled sample, that has been machined to exhibit an idealised two dimensional roughness pattern at its surface, was subjected to a Mach 5 turbulent boundary layer. Spatially resolved heat transfer data was collected utilising infrared thermography (IRT) adapted to account for the three dimensional effects that result from surface roughness. The heat transfer data was collected at blowing parameters 0-2.5, and molecular weights of 14-28 gmol^{-1} presented as an augmentation factor relative to the smooth, non injection case.

Keywords: *Hypersonic, Surface Roughness, Mass injection, Ablation*

Nomenclature

Latin

B_h – Blowing Parameter
c_p – Specific Heat Capacity
D – Empirical fitting parameter
F – Blowing Ratio
h – Enthalpy
k – Roughness Height
k – Thermal Conductivity
k^+ – Roughness Reynolds Number
K_D – Darcy Coefficient
K_F – Forchheimer Coefficient
M – Mach Number
M_r – Molecular Weight
n – Empirical fitting parameter
p – Pressure
$\dot{q}$ – Heat Flux
St – Stanton Number
T – Static Temperature
u – Velocity
x – Distance Along the Plate

Greek

ε – Emissivity
θ – Camera Angle
ν – Kinematic Viscosity
ρ – Density
τ – Shear Stress
ϕ – Porosity

Subscripts

∞ – Free Stream Quantity
$B_h = 0$ – No Gas Injection
e – Edge Condition
r – Recovery
$Rough$ – Rough wall value
s – Equivalent Sand-Grain Roughness
$Smooth$ – Smooth wall value
w – Wall Condition

1. Introduction

Hypersonic flight is an extremely taxing ordeal on a vehicle, specifically during the reentry phase of its trajectory [1]. The exchange of the kinetic energy of the vehicle with the internal energy of the flow produces extremely high temperatures and thus heat fluxes and heat loads. By far the most prevalent method to combat these high heat fluxes are ablative heat shields — a semi passive thermal protection system (TPS) that coats the external surface of the vehicle. In response to the high temperature environment, the material thermally decomposes into gaseous products and a porous char layer that further

[1]*Department of Engineering Science, Univeristy of Oxford, Parks Road Oxford, OX1 3PJ. Corresponding author email address: wesley.condren@eng.ox.ac.uk*

Copyright © 2024 by the author(s)

breaks down into more gaseous products via sublimation. These processes absorb energy that would have been incident on the vehicle surface and instead transfer it away. Moreover, the relativity cooler pyrolysis gases provide an additional cooling effect as they pass through the char layer into the boundary layer (colloquially known as blowing) thus maintaining subcritical outer wall temperatures.

The surface of an ablator facilitates a myriad of complex interactions and phenomena with strong implications on the subsequent behaviour of the heat shield. To ensure an efficient and effective thermal protection system and vehicle, understanding and predicting these phenomena are required prior to flight. This work focuses on the effect of the large scale roughness elements left as the material ablates in combination with the effect of blowing. The independent effects of roughness and blowing on heat transfer and skin friction are expected to be in competition. The roughness elements generated can be sufficiently large as to protrude into the sonic line of the boundary-layer, enhancing turbulent motions and consequently increasing the convective heat flux above smooth wall levels [2]. Whereas, the pyrolysis gases serve the same role as the coolant fluid in a transpiration cooled wall with the char layer acting as the porous material. The coolant fluid not only absorbs heat from the material as it passes through it but also generates a buffer between the surface and the high temperature gas which drives down the convective heat flux experienced by the surface [3]. Furthermore, mass injection reduces the skin friction experienced by the surface [4] which opposes the increase that results from surface roughness.

Research into each phenomena independently has been conducted as early as the 1930s and 50s with the pioneering work by Nikuradase [5] and Schlichting [6] on surface roughness and that by W.D.Rannie on porous wall cooling [7]. The transpiration cooling effects of the pyrolysis gases are typically understood through film theory put forward by Mickley [8] and later expanded to account for boundary layer state and coolant fluid by Moyer and Rindal [9]. It has since been further expanded to encapsulate the effects under hypersonic flow conditions by Naved *et.al* [10]. In contrast, very few studies address surface roughness effects, specifically large scale surface roughness effects, in a hypersonic flow environment and fewer still pertain to those effects in conjunction with blowing. The work by Wilder and Prabhu [11] investigates the effects of a patterned roughness modelling that seen on woven TPS. The roughness was mapped onto a 45° sphere-cone and subjected to Mach 9.68 hypersonic flow in the NASA Ames Hypervelocity Free Flight Aerodynamic Facility achieving roughness Reynolds numbers of 36-148. The heat flux data was evaluated from temperature distributions measured by IR thermography assuming semi-infinite condition. The data compared reasonably well with Powars' correlation using the roughness height based roughness Reynolds number but an alteration to Dirling's shape parameter was required to achieve the same agreement when using the equivalent sand-grain height. More recently, the work by Hambidge *et.al* conducted at the Oxford High Density tunnel on a flat plate at Mach 5 using a similar woven TPS roughness pattern as Wilder and Prabhu showed again that roughness height based roughness Reynolds number achieved a better agreement to Powars' than the equivalent sand grain approach. Moreover, it highlighted that the Reynolds analogy no longer holds for patterned roughness in hypersonic flow fields.

The main body of experimental work that investigates the combined effects of roughness and blowing is that by Holden *et.al* [12]. The experiments were conducted at Mach numbers of 11, 13 and, 15 on a 10.5 degree conical model. The model was instrumented with intricate patterned thin film, calorimeter and skin friction gauges that allowed gas to be injected through them, to measure the local heat flux and skin friction. The results showed that the overall augmentation in heat flux and skin friction are not a simple superposition of blowing and roughness effects. The same conclusion was reached by the supersonic work conducted by Voisinet at Mach 3 [13] and the earlier subsonic work by Healzer and Pimenta [14] [15].

This paper presents heat transfer over a rough transpiration cooled surface. The experiments were conducted in the Oxford High Density Tunnel (HDT) at Mach 5 with a flat plate model geometry. For the heat flux data, infrared thermography was used, having previously been successful in providing spatially resolved data over a purely transpiration cooled surface [10] and later adapted to account for the three-dimensional effects introduced by surface roughness [16]. The heat flux measurements were carried

Copyright © 2024 by the author(s)

out using an optical technique due to their ability to provide spatially continuous, two-dimensional data without introducing irregularities in the rough surface. The injected gases consisted of N_2 along side a mix of N_2 and He such that the average molecular weight equalled that of typical pyrolysis products at equilibrium at 2000K. The Stanton number augmentation of the combined cases for a range of blowing parameters are compared the superposition of current correlations.

2. Theoretical Approach

2.1. Pyrolysis Injection

In ablative research the effect of pyrolysis gas injection is typically understood though the simple film theory model proposed by Mickley [[17], [18], [19]]. Film theory states that the stanton number reduction experienced by the surface is predicted by means of an idealisation that restricts the transition from wall conditions to that in the free-stream to a thin laminar film [8]. Taking mass, momentum and energy balances over the film the model arrives at Eq. (1).

$$\frac{St}{St_{B_h=0}} = \frac{B_h}{e^{B_h} - 1} \tag{1}$$

Where $St_{B_h=0}$ is the uncooled stanton number and B_h is the blowing parameter, a non dimensional mass transfer rate, defined in Eq. (2).

$$B_h = \frac{F}{St_{B_h=0}} \tag{2}$$

F is the blowing ratio defined as the ratio between the coolant mass flux and that at the boundary layer edge

$$F = \frac{\rho_f u_f}{\rho_e u_e} \tag{3}$$

Simple film theory does not take into count the state of the boundary layer over the porous medium nor does it account for the effects introduced by foreign gas injection. The prior is usually addressed with a correction factor λ (commonly taken as 0.5 or 0.8 for turbulent flows) that augments the blowing parameter in Eq. (1) as shown in Eq. (4)[9]. Correcting film theory for foreign gas injection is primarily done through a correction factor defined by the ratio of molecular weights of the free stream and injected gas $\left(\frac{M_{r_e}}{M_{r_f}}\right)$ [20] [21].

$$\frac{St}{St_{B_h=0}} = \frac{\lambda \cdot B_h}{e^{\lambda \cdot B_h} - 1} \tag{4}$$

Lastly, film theory assumes that the porous medium is of infinite length. In the context of ablative it is unlikely that the out-gassing of pyrolysis products is constant over the whole surface and thus in this work is modelled as a finite rough walled porous injector. In order to account for the development of the boundary layer over the surface as gas is injected the factor in Eq. (5) further augments the blowing parameter raised to the power of 0.8 for turbulent flows [22].

$$\left[\frac{x - x_s}{x}\right]^{0.8} \tag{5}$$

Where x_s is the location of the start of the injector along the flat plate.

Applying each correction to Mickley's film theory results in the correlation laid out in Ref.[10] shown in Eq. (6)

Copyright © 2024 by the author(s)

$$\frac{St}{St_{B_h=0}} = \frac{\omega}{e^{\omega} - 1} \tag{6}$$

Where ω is as follows

$$\omega = D \cdot B_h \cdot \left[\frac{x - x_s}{x}\right]^{0.8} \cdot \left[\frac{M_{r_e}}{M_{r_f}}\right]^{n} \tag{7}$$

Where D and n are fitting parameters. In a Mach 6 turbulent boundary layer D and n were found to be 3 and 1.4 respectively [10].

2.2. Surface Roughness

Surface roughness can result in an increase in local heat flux and shear stress as well as introduce early boundary layer transition. The effects of patterned or random surface roughness have been understood typically though the concept of 'equivalent sand-grain roughness' introduced by Schlichting [6] using the experimental work of Nikuradase [5]. Schlichting states that any roughness geometry can be characterised by a single length scale k_s — the equivalent sand grain roughness height. This height,k_s, as summarised in Ref.[23] is the height of a sphere for a uniform, idealised Nikuradse-like sand-grain roughness that has the same effects on the flow field as the patterned or random roughness. There are various methods to evaluate the k_s from the actual roughness height k most notably Dirling [24], Sigal & Danberg [25] and van Rij *et.al* [26].

A roughness Reynolds number is then defined to correlate the influence of roughness on the external flow field defined as shown in Eq. (8)

$$k_s^+ = \frac{k_s u_\tau}{\nu} \tag{8}$$

Where u_τ is the friction velocity

$$u_\tau = \sqrt{\frac{\tau_w}{\rho}} \tag{9}$$

The prediction of the augmentation in heat flux as a result of roughness in compressible flows is done largely through Powars' correlation [27] developed using experimental data collected during the PANT project [28] defined in Eq. (10).

$$\left(\frac{St_{Rough}}{St_{Smooth}}\right)_{B_h=0} = \frac{2}{3} \cdot log_{10}\left(k_s^+\right) + \frac{1}{3} \tag{10}$$

Note that, although the use of equivalent sand-grain roughness is common practise, there is discussion of its validity in the context of large scale roughness in hypersonic flows. The work by Hambidge *et.al* [29] showed that agreement to Powars' correlation is highly sensitive to the definition of k^+ used. As there is currently a lack of correlations that pertain to large scale roughened surfaces in hypersonic boundary layers this work will maintain the use of Powars.

3. Experimental Set Up

3.1. Oxford High Density Wind

The experiments were conducted in the High Density Tunnel (HDT), a heated Ludwieg tube, at the Oxford Thermo-fluids Institute. The HDT is a low enthalpy short duration facility with the capability to produce high unit Reynolds number flows typically ranging between Mach 4 and 7. When operating in Ludwieg mode, HDT produces several periods of the order of tens of milliseconds with steady total pressure and unit Reynolds numbers. A more thorough breakdown of the operation and function of HDT can be found in [30] [31].

Copyright © 2024 by the author(s)

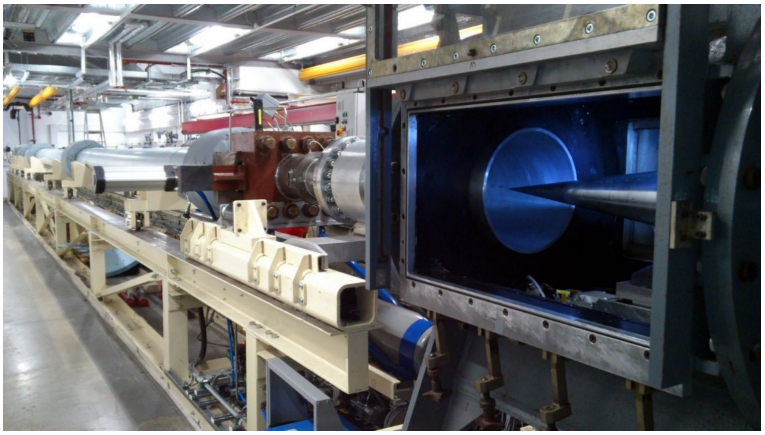

Fig 1. The Oxford High Density Tunnel with a conical model in the test section.

3.2. Test Conditions

The conditions used during the experiment are detailed in Table 1 with a combination of sutherland and Keyes laws developed by NASA used to determine viscosity. Operation produced these steady conditions with unit Reynolds numbers between 32 and 48 million per meter with nitrogen as the free stream gas.

Parameter	Unit	Condition 1	Condition 2	Condition 3
T_e	K	74	72	71
p_e	kPa	6.2	5.0	4.0
ρ_e	kgm^{-3}	0.28	0.23	0.20
u_e	ms^{-2}	896	881	871
M_e	$-$	5	5	5
$Re_u\ (\times 10^6)$	m^{-1}	48	40	32

Table 1. Boundary layer edge flow properties.

3.3. Model

The test piece shown in Fig.2 is a vertically mounted 575x260x60 mm flat plate. A boundary layer trip of height 0.5mm is placed 67.5mm downstream of the sharp leading edge followed by a Thin Film Gauge (TFG) array, used to characterise the state of the incoming boundary layer 85mm downstream of the leading edge. The plate houses a test article 205mm downstream if the leading edge with dimensions 290x90mm. Both the TFG-array and test article are centred about the flat plate's mid point.

The model is instrumented with eight Honeywell pressure sensors on the flat surface to monitor the progression of edge effects along the plate. Additionally, two Kulites measure the static pressure of the flow 15 mm prior to the test article. To ensure the model is aligned with the oncoming flow, an angle of attack probe with five Kulites, four positioned axially symmetric around the probe and one positioned centrally to measure pitot pressure, is used. Along side this a twin probe, provides an additional pitot pressure measurement as well as a total temperature measurement with an aspirated thermocouple.

Copyright © 2024 by the author(s)

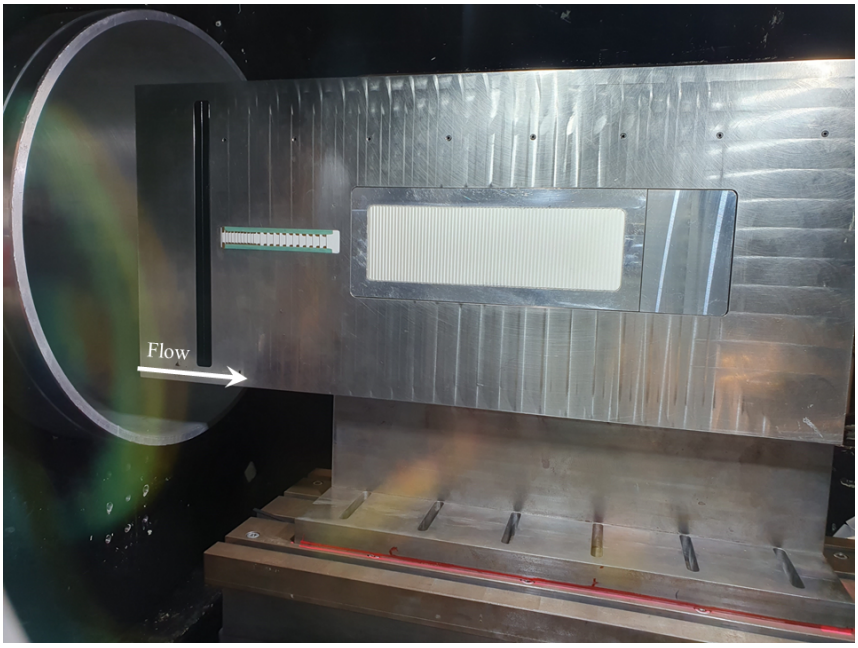

Fig 2. Flat plate model with porous injector mounted in the HDT test section.

3.4. Porous Injector & Roughness Geometries

The porous material used in this work is METAPOR CE170, a commercially available micro-porous material consisting of aluminium hydroxide bonded with resin with a mean pore diameter of 20μm. The material properties of METAPOR are summarised in Table 2. The thermal properties and material density were evaluated externally by *NETZSCH* from multiple samples of the material. The Darcy-Forchheimer coefficients were evaluated in-house using the setup described in Ref.[32] and the emissivity was evaluated in-house in a radiation shield environment [33].

Parameter	Symbol	Value
Porosity	ϕ	0.20
Density	ρ	1.18 gcm^{-3}
Specific Heat Capacity	c_p	1.408 Jg^{-1}K^{-1}
Thermal Conductivity	k	0.175 Wm $^{-1}$K^{-1}
Thermal Product	$\sqrt{\rho c k}$	1829 Jm^{-2}K^{-1}s$^{-\frac{1}{2}}$
Darcy Coefficient	K_D	1.86$\times 10^{-13}$ m^2
Forchheimer Coefficient	K_F	7.44 $\times 10^{-9}$ m
Normal Emissivity	ε	0.95

Table 2. METAPOR CE170 material properties.

The roughness geometry chosen was an idealised two dimensional saw-tooth pattern with a windward angle of 25 degrees, a leeward angle of 80° and, a roughness height of 1mm. A height map is shown in Fig.3 and Table.3 summarises the geometric details including the calculated k_s values using Diriling, Sigal and Van Rij corrleations [[24],[25],[26]]. The pattern was machined directly out of the METAPOR CE170 material. Fig.4 shows the rough porous injector sealed into an aluminium cover-plate which secures the injector to the flat plate model as well as a smooth porous piece that was machined to serve

Copyright © 2024 by the author(s)

as the control.

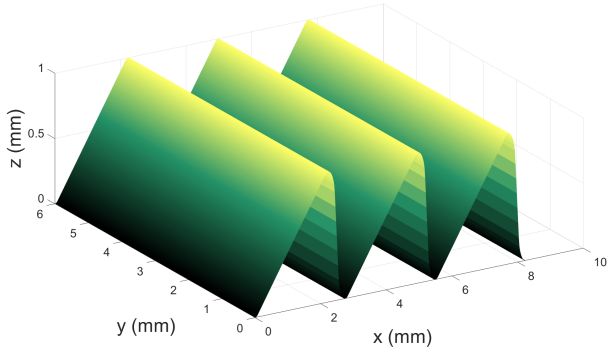

Fig 3. Surface Geometry for the idealised 2D saw-tooth roughness pattern.

Parameter	Unit	Value
θ_{ww}	deg	25
θ_{lw}	deg	80
k	mm	1
$k_s(Dirling)$	mm	5.54
$k_s(Sigal)$	mm	8.00
$k_s(vanRij)$	mm	1.94

Table 3. Saw-tooth pattern details.

(a) **(b)**

Fig 4. (a) Pictures of smooth and rough surfaces.

4. IR Thermography

The heat flux experienced by the surface was measured utilising infra-red thermography (IRT). As the porous sample cannot be easily instrumented and large-scale roughened surfaces requiring patterned TFGs and/or calorimeters, the non-intrusive nature of the IRT allows for spatially resolved measurements directly on the rough injector's surface [29] [4]. The IR data in this experiment was collected using a *Telops* M3K FAST mid-wave infrared camera with a 100mm focal length lens through a 100mm diameter

Copyright © 2024 by the author(s)

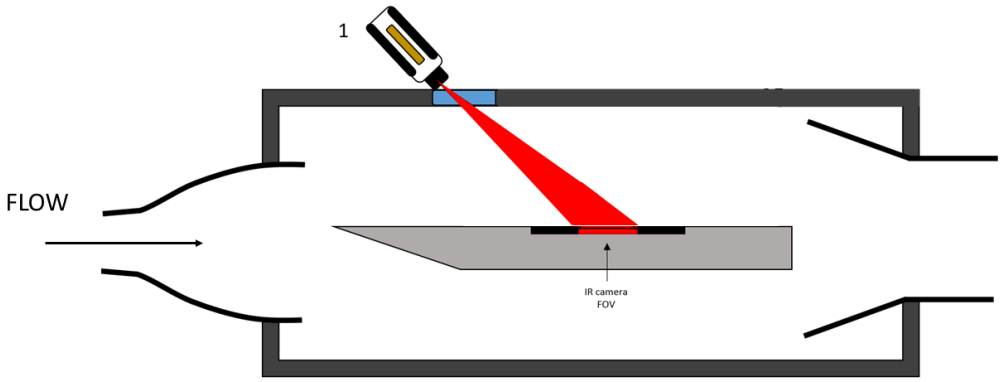

Fig 5. Schematic showing the position of the IR camera relative to the flat plate model during the experimental campaign

anti reflection coated sapphire window. The FoV of the set up covered a region 265-310mm downstream of the sharp leading edge and $\pm$22mm about the centre line of the flat plate. The resulting resolution at the surface was 0.14 mm per pixel. A schematic of the set is shown in Fig.5

The raw data from the IR camera was processed first by applying a black body calibration, relating counts to an equivalent black body temperature, on a pixel by pixel bases. The calibration was conducted in-situ with the CI-Systems SR-33-7 calibrator placed in the same position as the flat plate model during the test. Next, an emissivity correction was applied using the experimentally determined emissivity of METAPOR CE170, converting the data to the true body temperature. Both the black body calibration and emissivity correction are described in more depth by Naved *et.al* [33].

Due to the directional dependence of the material's emissivity, the view angle of the camera,θ_v, must be determined. For large scale roughened surfaces the relative view angle is a function of both the angle of the camera relative to the flat surface θ_{flat} and the local angle of rough surface geometry θ_{Rn} displayed in Eq. (11) [16]. As the saw-tooth geometry is known accurately prior to testing only the camera position in the world frame of reference is needed.

$$\theta_v = \theta_{flat} \pm \theta_{Rn} \tag{11}$$

The θ_{flat} distribution was determined using a target plate placed in the same plane as the rough porous injector with 1 mm holes spaced equally 2.5 mm apart backed by aluminium with a matte black finish to enhance the contrast of the holes in the IR spectrum. Full details of the methodology are found in Ref.[16]. During this experiment the angles to the surface once augmented by θ_{Rn} were well below 20° resulting in a very uniform emissivity over the FoV.

Once the corrected temperature profile was obtained and the change in temperature over the test time was evaluated, the heat flux, $\dot{q}_{IR}$, was determined using Oldfield's method [34]. This assumes semi-infinite conduction which does not take into account the curvature effects of the 200μm fillet at the peaks and troughs of the saw-tooth pattern. Future work will address the three-dimensional conduction effects on rough surfaces.

Lastly the data was converted to stanton number by normalising by the boundary layer edge properties

Copyright © 2024 by the author(s)

as shown in Eq. (12)

$$St = \frac{\dot{q}_{IR}}{\rho_e u_e \left(h_r - h_w\right)} \tag{12}$$

Where ρ_e, u_e and h_w are the free stream density, free stream velocity and wall enthalpy respectively. h_r is the recovery enthalpy is found as per Eq. (13)

$$h_r = c_{p_e} T_e \cdot \left[1 + r\left(\frac{\gamma + 1}{2}\right) \cdot M_e^2\right] \tag{13}$$

Where r is the recovery factor taken as $r = Pr^{\frac{1}{3}}$ for turbulent flows.

5. Results & Discussion

The magnitude of the IR data was validated against the turbulent Eckert heat flux correlation [35]. Figure.6 shows a span-wise average of the stanton number plot over 20 mm centred about the flat plate mid point for condition 2. The Eckert line has been shifted to the location of the boundary layer trip.

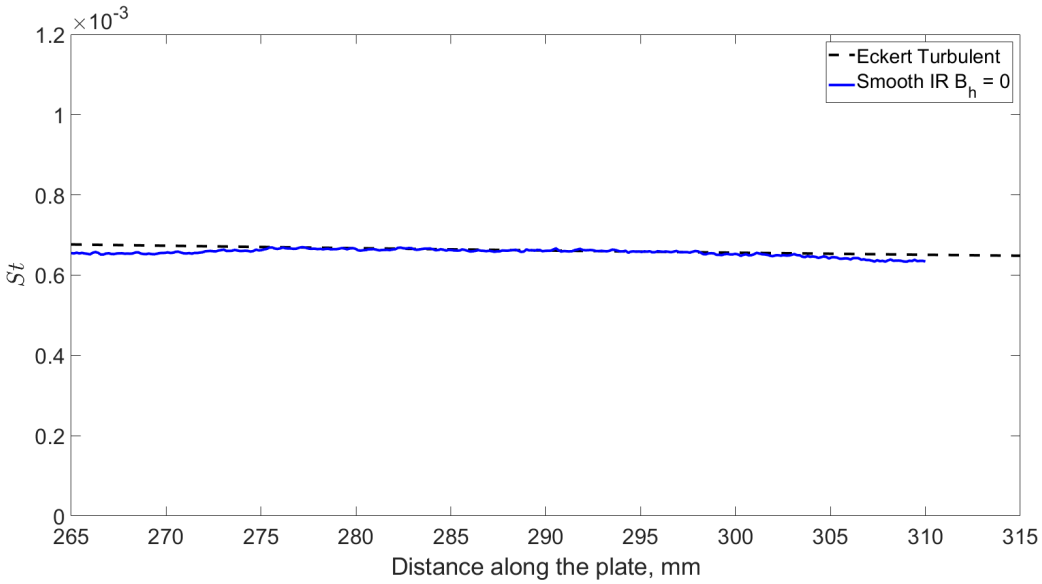

Fig 6. Comparison of measured Stanton number on a smooth plate with the Turbulent Eckert correlation.

The absolute magnitude of the IR data is in good agreement with this Eckert correlation at the centre of the FoV deviating at the outer edges. As a result of this deviation the span-wise and area averaged results shown below are taken between 275-300mm along the plate.

For the both the smooth and rough injection cases a blowing parameter, B_h, of 0.8 was tested with nitrogen and Nitrogen/Helium mix and a B_h of 2.5 was investigated using nitrogen only.

5.1. Smooth Data

Figure.7 shows the stanton number reduction maps calculated by normalising the Stanton number evaluated for the injection case by that of the smooth non blowing case at condition 2.

Copyright © 2024 by the author(s)

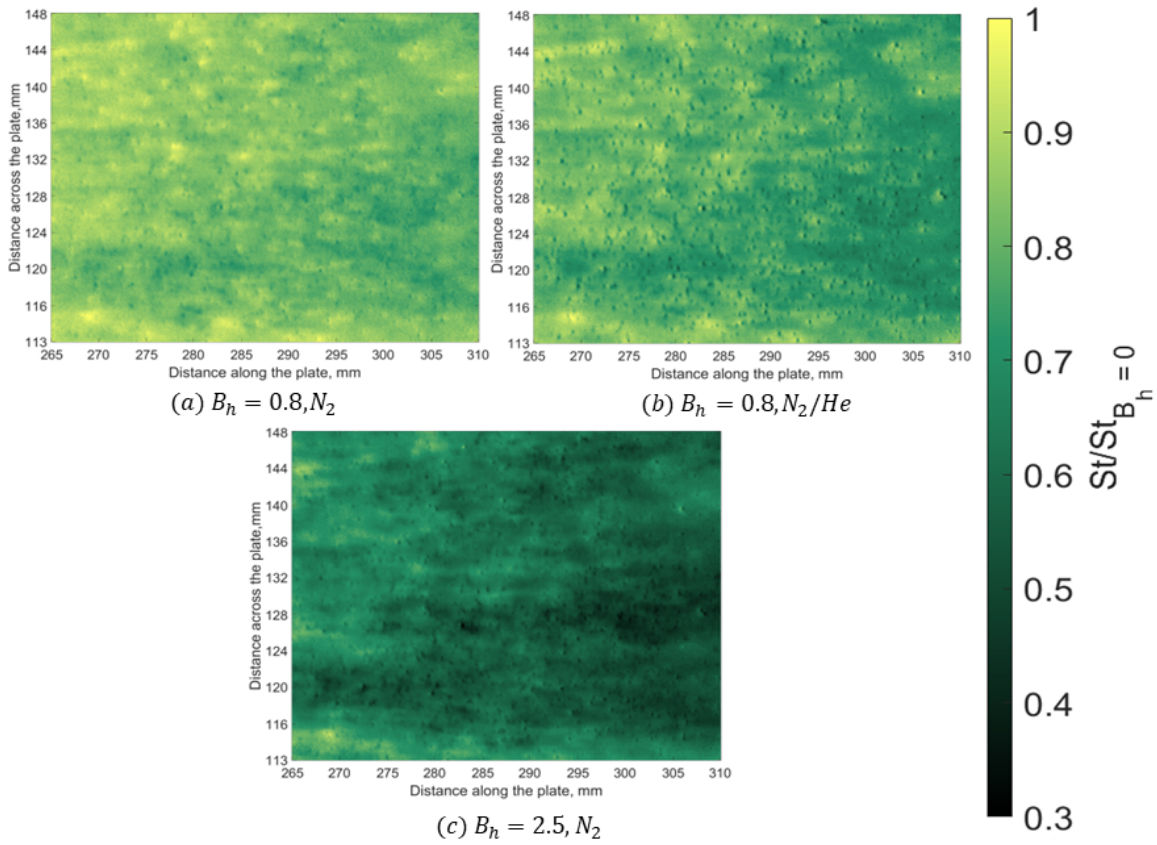

Fig 7. Stanton number reduction contours on the smooth porous injector calculated at the two blowing ratios and using different gases at condition 2.

As expected the reduction increases with an increasing blowing parameter B_h and with a decrease in gas molecular weight highlighted again in the span-wise average line plots in Fig.8.

Figure.9 shows the data compared to the modified Mickley and Moyer-Rindal correlation in Eq. (6) that counts for the development of the boundary layer over the finite injector and the increase in blockage effect accompanied by a lower molecular weight gas. Each point represents a span wise average at a particular distance along the plate. The constants D and n where chosen as 1.05 and 0.6 respectively to achieve a good fit to the experimental data. The value of n selected in this work fits within the range 0.5-1 reported in previous transpiration cooling works for turbulent flows [20] [36] and translates to a 40% increase in cooling effect compared to the Nitrogen injection case.

Copyright © 2024 by the author(s)

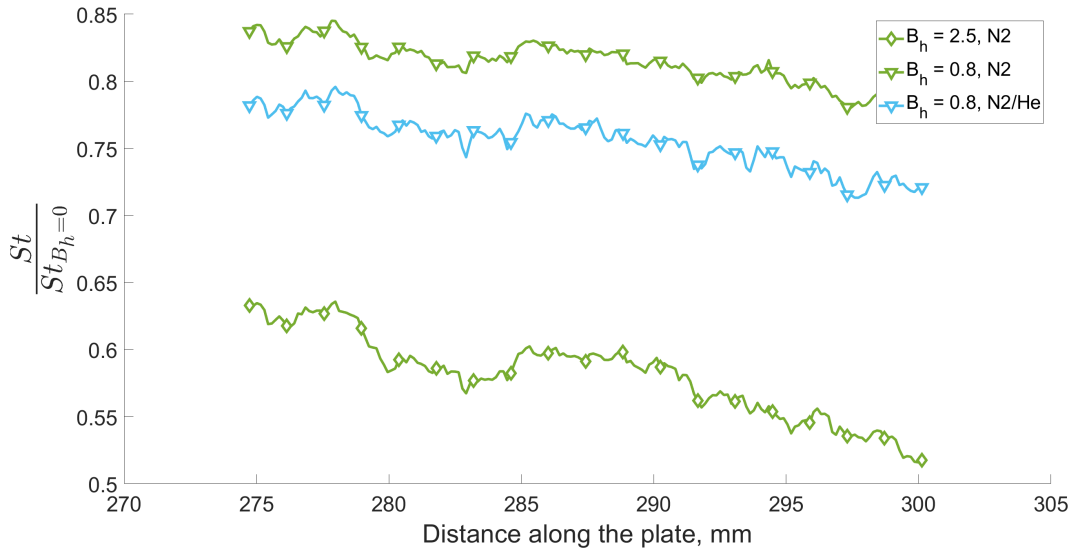

Fig 8. Span-wise averaged Stanton number reduction along the porous injector at condition 2.

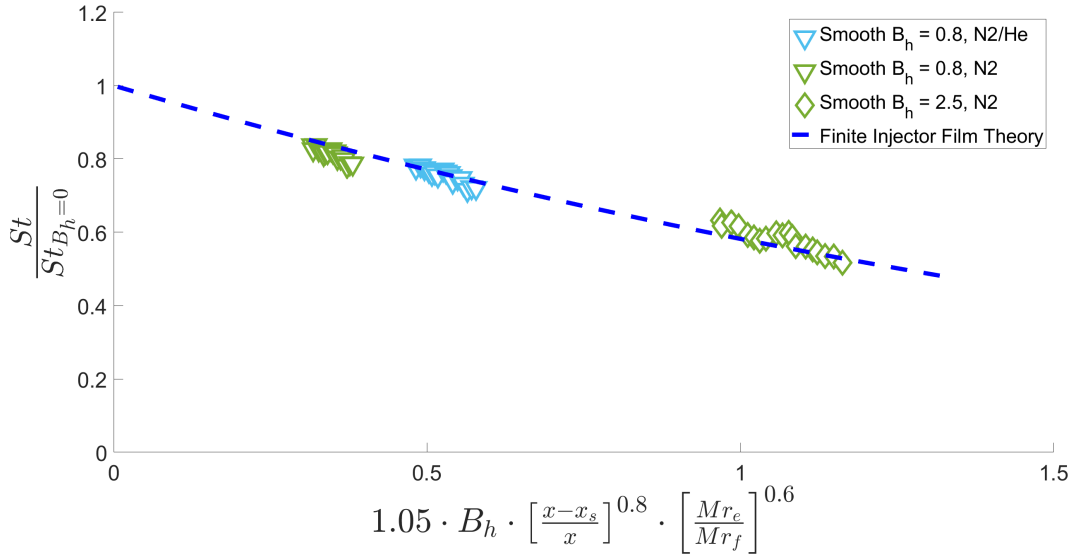

Fig 9. Span-wise averaged Stanton number reduction along the smooth porous injector verse the blowing parameter, B_h.

5.2. ST25 Data

The contour plots for each B_h value and injected gas are shown in Fig.10 for condition 2. This shows a maximum heat flux augmentation of 2.2 at the peaks and a minimum of 0.7 at the troughs of the saw-tooth pattern diminishing to 1.1 and 0.4 respectively with nitrogen injection at a blowing parameter of 2.5. This result maintains the expected trend of an increase in cooling effect as the blowing parameter is increased as shown in the smooth injection cases reported in section 5.1.

Copyright © 2024 by the author(s)

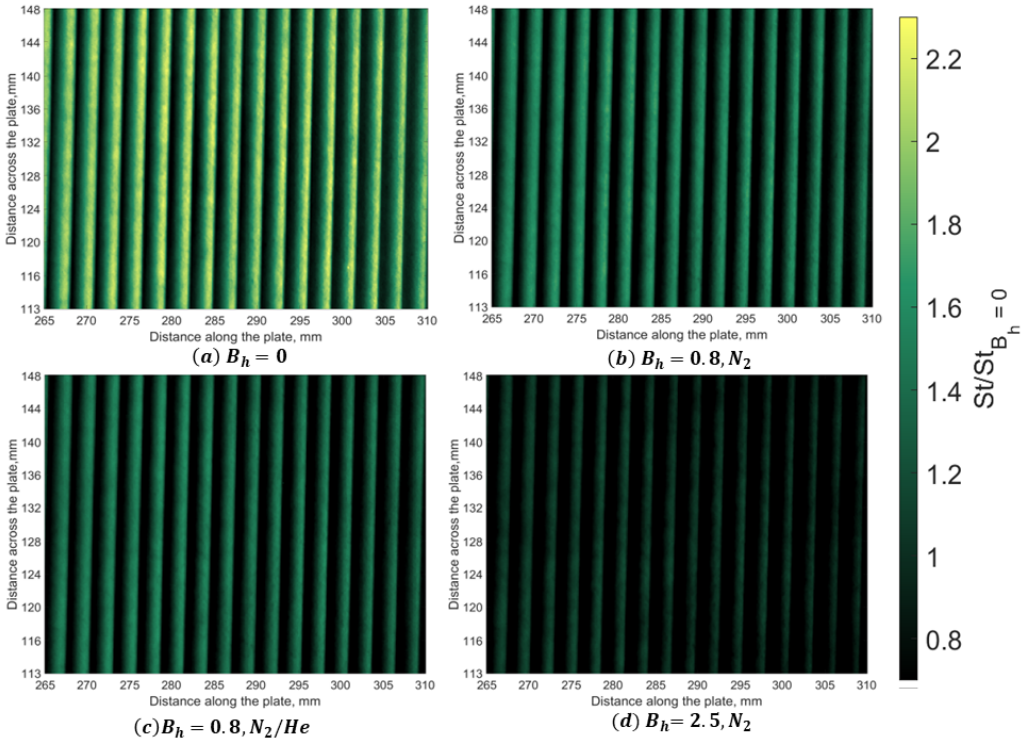

Fig 10. Stanton number reduction contours for ST25 rough porous injector calculated at the two blowing ratios and using different gases.

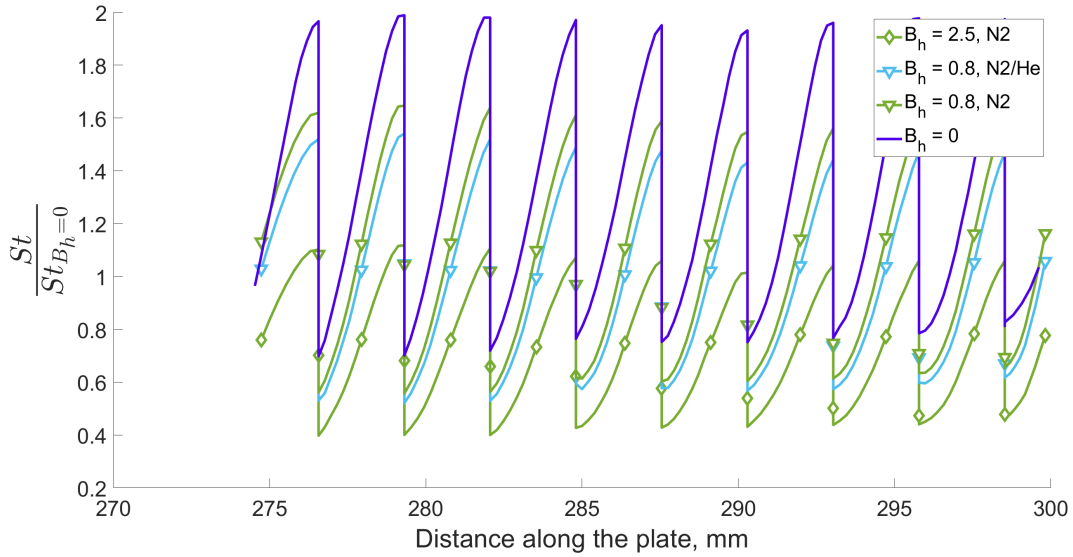

Fig 11. Span-wise averaged Stanton number reduction along the rough porous injector verse the blowing parameter, B_h.

Figure.12 shows the average ratio between the heat flux experienced at the peak of the sawtooth geometry to that at the troughts for each rough wall case. Interestingly, the ratio between the two remains fairly constant across each case varying by less than 4% of the non injection case at the

Copyright © 2024 by the author(s)

highest blowing blowing parameter reduction to less than 2% at a B_h of 0.8.

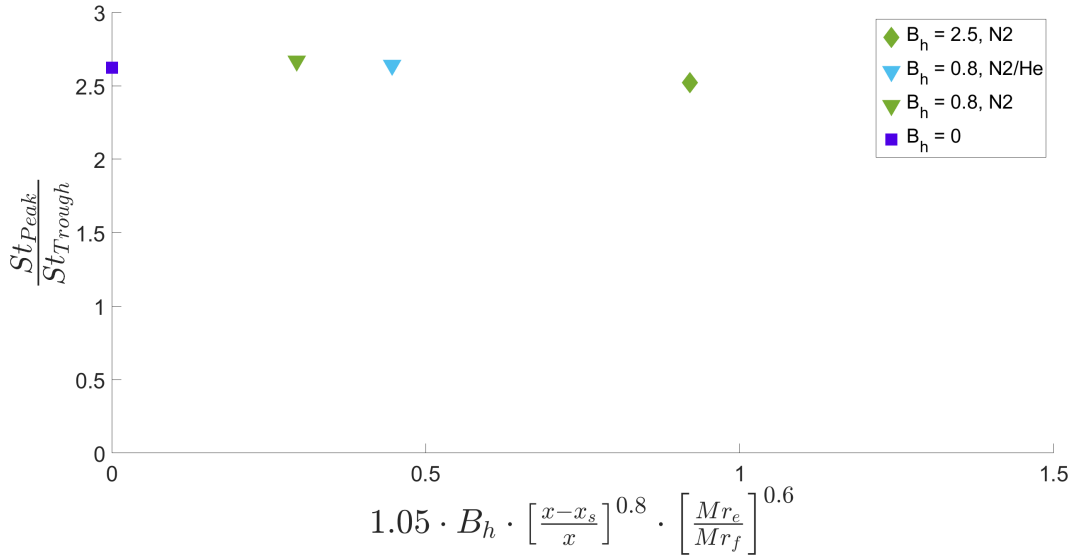

Fig 12. Ratio of average Stanton number at peaks (St_{Peak}) to that at the troughs (St_{Tough}) of the Sawtooth pattern agains the modified blowing parameter

The area averaged Stanton number augmentation over the smooth wall control ($B_h = 0$) for both smooth and rough injection cases at condition 2 are plotted against the finite injector film theory correlation superimposed with the Stanton number enhancement predicted by Powars' in eq. (10). Two methods of superposition are used, the direct multiplication of the blowing and rough wall heat flux augmentation shown in Eq. (14) and the summation of the two shown in Eq. (15) [37].

$$\left(\frac{St}{St_{B_h=0}}\right) \times \left(\frac{St_{Rough}}{St_{Smooth}}\right)_{B_h=0} \tag{14}$$

$$1 + \left[\left(\frac{St}{St_{B_h=0}}\right) - 1\right] + \left[\left(\frac{St_{Rough}}{St_{Smooth}}\right)_{B_h=0} - 1\right] \tag{15}$$

The value of the roughness Reynolds number was calculated using the actual roughness height, k, and an equivalent sand-grain roughness height, k_s, defined using van Rij's correlation. It can be seen that the simple superposition by either addition or multiplication of the two effects fails to capture the overall augmentation seen in all four of the rough wall injection cases with the k^+ value calculated with the actual roughness height fairing better than the equivalent roughness height. Additionally, the direction multiplication method yields magnitudes that agree more with the data than the summation method.

Figure.14 shows the area averaged rough-wall Stanton number enhancement for all four ST25 injection cases (Stanton number enhancement above the respective smooth wall injection case) against Powars' with the roughness Reynolds number similarly calculated with k and k_s mentioned above including Dirling and Sigal sand grain roughness heights. This result seconds the findings in Hambidge *et.al* [29] that evaluating k^+ using the actual roughness height shows better agreement with Powars' than that calculated with an equivalent sand-grain height. Secondly, it can be seen that with an increase in the blowing parameter from 0 to 2.5 the observed rough wall augmentation diminished by 10%. Interestingly, the nitrogen helium mix data shows a slightly smaller reduction in rough wall augmentation than the nitrogen injection at the same B_h.

Copyright © 2024 by the author(s)

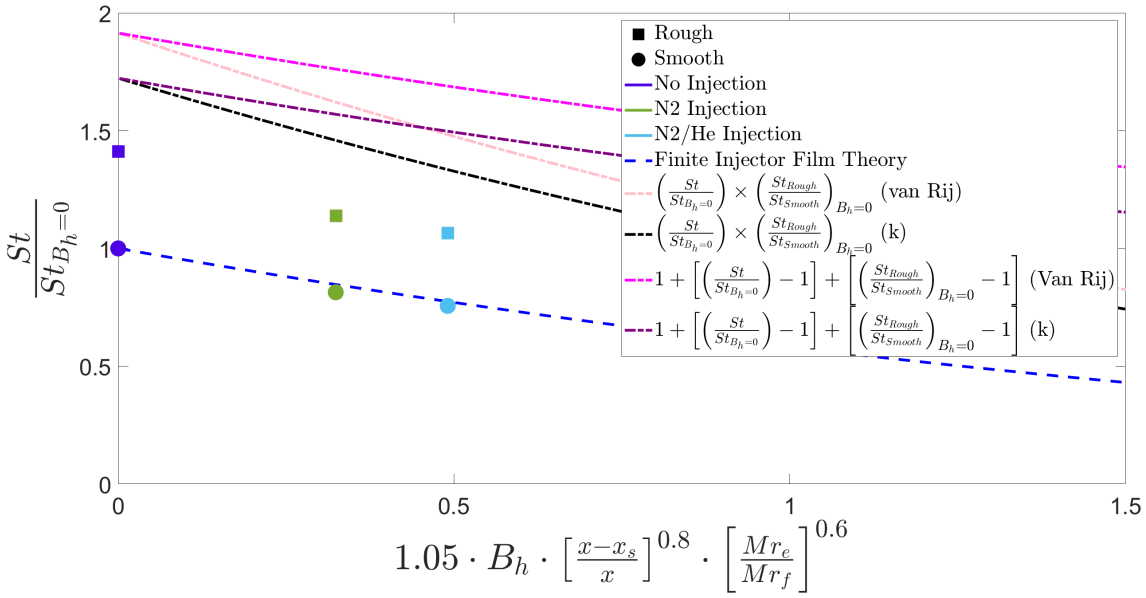

Fig 13. Area averaged Stanton number augmentation for both smooth and rough wall injectors vs finite injector film theory augmented by Powars Stanton number enhancement for a given k^+.

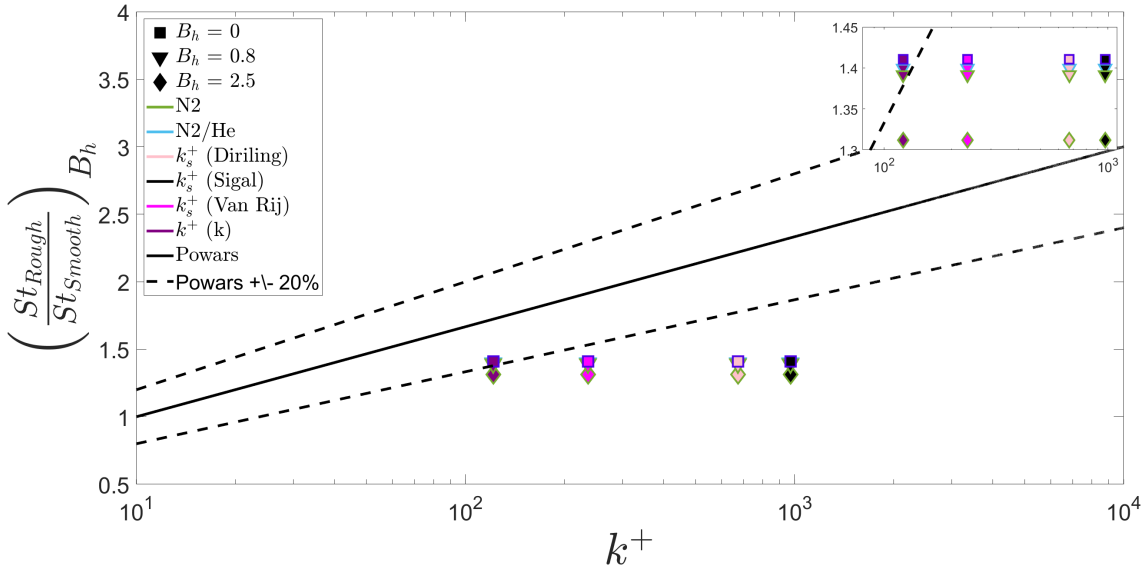

Fig 14. Area averaged Stanton number enhancement above respective smooth wall injection case for rough wall injectors against Powars' for a given k^+.Here St_{Smooth} refers to the respective smooth wall injection case.

6. Conclusion

An experimental investigation of the combined heat flux augmentation experienced by a large scale roughened surface with blowing has been performed at Mach 5 with Reynolds numbers ranging from 30 to 50 million per metre in the Oxford High Density tunnel. The roughness geometry was an idealised two dimensional saw-tooth pattern with a roughness height of 1mm. Nitrogen and a nitrogen/helium mix modelling pyrolysis gases at 2000°C were used as coolants at blowing parameters ranging from 0 to 2.5 The heat flux data over the surface of the porous injectors was measured using IR thermography.

Copyright © 2024 by the author(s)

The smooth injection case data was found to agree with the modified film theory presented in Ref.[10] that accounts for the development of the boundary over the injector surface as well as the change in blockage effect introduced by foreign gas injection. The nitrogen helium mixture exhibited a 40% increase in cooling effectiveness over the nitrogen gas. Additionally, the combined roughness and blowing data showed that the simple superposition of rough wall and blowing heat flux augmentations does not accurately predict the overall augmentation of combined problem found in ablatives, supporting the conclusions of Holden *et.al.* [12]. Furthermore, a decrease in the rough wall heat flux augmentation was found with an increase in injected mass flux and curiously the lighter gas mixture was found to diminish the enhancement by a smaller degree than nitrogen although more data is required to draw a meaningful conclusion on this.

Future experimental work with a finer selection of blowing parameter and a varied set of coolant gases will provide further insight into the combined effects of roughness and blowing in abaltive heat shields and allow for correlations to be developed that capture these effects over a wider range of conditions.

7. Acknowledgements

The authors would like to thank Tristan Crumption for the operation of the Oxford High Density Tunnel without which this work would not be possible. The authors thank Dr Jim Merrifiled and those Fluid Gravity Engineering for their insightful advice.

References

[1] J.D.Anderson: Hypersonic and High Temperature Gas Dynamics (1983)

[2] Neeb, D., Gülham, A., Merrifield, J.A.: Rough-Wall Heat Flux Augemtation Analysis Within the ExoMars Project. Journal of Spacecraft and Rockets, 163(1) (2016)

[3] Rubesin, M.W.: The Influence of Surface Injection on Heat-Transfer and Skin Friction Associated With the High-Speed Turbulent Boundary Layer (1956). URL https://digital.library.unt.edu/ark:/67531/metadc62139/:

[4] Holden M S., L.G., Millikan, C.B.: A simplified theory of porous wall cooling (1994). URL https://ntrs.nasa.gov/citations/19940030459

[5] Nikuradse, J.: Law of flows in rough pipes, English Translation. NACA TM 1292 (1950)

[6] Schlichting, H.: Experimental Investigation of the problem of surface roughness (1936)

[7] Rannie, W., Dunn, L.G., Millikan, C.B.: A simplified theory of porous wall cooling (1947). URL http://dx.doi.org/2014/45706

[8] Mickley, H.S., Ross, R.C., Squyers, A.L., Stewart, W.E.: Flow Over a Flat Plate With Blowing or Suction. NACA TN 3208 (1954). URL https://digital.library.unt.edu/ark:/67531/metadc57322/

[9] Moyer, C.B., Rindal, R.: An analysis of the coupled chemically reacting bounday layer and charring ablator. Part 2- Finite difference solution for the in-depth response of charring materials considering surface chemical and energy balances. NACA CR-1061 (1968)

[10] Naved, I., Hermann, T., Hambidge, C., Ifti, H.S., Falsetti, C., McGilvray, M.: Transpiration Cooling Heat Transfer Experiments in Laminar and Turbulent Hypersonic Flows. AIAA (2022)

[11] Wilder, M.C., Prabhu, D.K.: Rough-Wall Turbulent Heat Transfer Experiments in Hypersonic Free Flight (2019). URL http://dx.doi.org/10.2514/6.2019-3009

[12] Holden, M., Wadhams, T.P., Mundy, E.P.: A Review of Experimental Studies of Surface Roughness and Blowing on the Heat Transfer and Skin Friction to Nosetips and Slender Cones in High Mach Numbers Flows (2008). URL http://dx.doi.org/10.2514/6.2008-3907

Copyright © 2024 by the author(s)

[13] VOISINET, R.: Combined influence of roughness and mass transfer on turbulent skin friction at Mach 2.9 (1979). URL http://dx.doi.org/10.2514/6.1979-3

[14] HEALZER, J., MOFFAT, R., KAYS, W.: The turbulent boundary layer on a porous, rough plate - Experimentalheat transfer with uniform blowing. URL http://dx.doi.org/10.2514/6.1974-680

[15] Pimenta, M.M., Moffat, R.J., Kays, W.M.: The turbulent boundary layer: An experimental study of the transport of momentum and heat with the effect of roughness. Interim Report Stanford Univ., CA. Thermosciences Div. (1975)

[16] Condren, W.J., Hambidge, C., Steuer, D.C., Naved, I., McGilvray, M.: A Method for IR Measurement of Large Scale Roughened Surfaces in Hypersonic Flow (2023). URL http://dx.doi.org/10.2514/6.2023-2443

[17] Amar, A.J., Blackwell, B.F., Edwards, J.R.: One-Dimensional Ablation Using a Full Newton's Method and Finite Control Volume Procedure. Journal of Thermophysics and Heat Transfer, 22(1):71–82 (2008). URL http://dx.doi.org/10.2514/1.29610

[18] D.Bianchi: Modeling of Ablation Phenomena in Space Applications. Ph.D. thesis, Spaienza University of Rome (2006)

[19] M.E.Ewing, T.S.Laker, D.T.Walker: Numerical Modelling of Ablation heat Transfer. Journal of Thermophysics and Heat Transfer, 27(4):615–632 (Oct 2013). URL http://dx.doi.org/10.2514/1.T4164

[20] Holden, M., Sweet, S.: Studies of transpiration cooling with shock interaction in hypersonic flow. URL http://dx.doi.org/10.2514/6.1994-2475

[21] MARVIN, J.G., POPE, R.B.: Laminar convective heating and ablation in the Mars atmosphere. AIAA Journal, 5(2):240–248 (1967). URL http://dx.doi.org/10.2514/3.3948

[22] Stalmach, C.J., J. J, B., Pope, T.C., McCloskey, M.H.: A Study of Boundary Layer Transition on Outgassing Cones in Hypersonic Flow (1971)

[23] Kadivar, M., Tormey, D., McGranaghan, G.: A review on turbulent flow over rough surfaces: Fundamentals and theories. International Journal of Thermofluids, 10:100077 (2021). URL http://dx.doi.org/https://doi.org/10.1016/j.ijft.2021.100077

[24] R. DIRLING, J.: A method for computing roughwall heat transfer rates on reentry nosetips. 8th Thermophysics Conference. AIAA (2005). URL http://dx.doi.org/10.2514/6.1973-763

[25] Sigal, A., Danberg, J.E.: New correlation of roughness density effect on the turbulent boundary layer. AIAA Journal, 28:554–556 (1990). URL http://dx.doi.org/10.2514/3.10427

[26] van Rij amd B J Belnap, J.A., Ligrani, P.M.: Analysis and Experiments on Three-Dimensional, Irregular Surface Roughness. Journal of Fluids Engineering, 124(3):671–677 (2002). URL http://dx.doi.org/10.1115/1.1486222

[27] Powars, C.A.: Passive Nosetip Technology (PANT) Program, Interim Report, Vol. III Part II - Roughness Augmented Heating Data Correlation and Analysis (1974)

[28] Wright, M., Edquist, K., Tang, C., Hollis, B., Krasa, P., Campbell, C.: A Review of Aerothermal Modeling for Mars Entry Missions (2010). URL http://dx.doi.org/10.2514/6.2010-443

[29] Hambidge, C., Steuer, D.C., Condren, W.J., McGilvray, M.: Roughness Induced Heat Transfer and Shear Stress Augmentation Measurements of the HEEET Thermal Protection System (2024). URL http://dx.doi.org/10.2514/6.2024-0444

[30] Wylie, S., Doherty, L., McGilvray, M.: Commissioning of the Oxford High Density Tunnel (HDT) for boundary layer stability measurements at Mach 7. 2018 Fluid Dynamics Conference. American Institute of Aeronautics and Astronautics (2018)

Copyright © 2024 by the author(s)

[31] McGilvray, M., Doherty, L.J., Neely, A.J., Pearce, R., Ireland, P.: The Oxford High Density Tunnel. 20th AIAA International Space Planes and Hypersonic Systems and Technologies Conference. AIAA (2015). URL http://dx.doi.org/10.2514/6.2015-3548

[32] Ifti, H.S., Hermann, T., McGilvray, M.: Flow Characterisation of Transpiring Porous Media for Hypersonic Vehicles (2018). URL http://dx.doi.org/10.2514/6.2018-5167

[33] Naved, I., Hermann, T., McGilvray, M., Rocher, M.E., Hambidge, C., Doherty, L., Page, L.L., Grossman, M., Vandeperre, L.: Heat Transfer Measurements of a Transpiration Cooled Stagnation Point in Transient Hypersonic Flow. AIAA, 53 (2020)

[34] Oldfield, M.L.G.: Impulse Response Processing of Transient Heat Transfer Gauge Signals. Journal of Turbomachinery, 130(2):021023 (2008). URL http://dx.doi.org/10.1115/1.2752188

[35] Eckert, E.R.G.: Engineering Relations for Heat Transfer and Friction in High-Velocity Laminar and Turbulent Boundary-Layer Flow Over Surfaces With Constant Pressure and Temperature. Transactions of the American Society of Mechanical Engineers, 78(6):1273–1283 (2022). URL http://dx.doi.org/10.1115/1.4014011

[36] Pappas, C.C., Okuno, A.F.: The Relation between Skin Friction and Heat Transfer for Compressible Turbulent Boundary Layer with Gas Injection (1965)

[37] Forsyth, P.R., hambidge, C., McGilvray, M.: Experimental Assessment of Hypersonic Comvective Heat Transfer Augmentation Due to Surface Roughness. Journal of Thermophysics and Heat Transfer, 38(2) (2024). URL http://dx.doi.org/10.2514/1.T6893

Copyright © 2024 by the author(s)